**NASA TECHNICAL MEMORANDUM**

NASA TM X-52860

NASA TM X-52860

# DEPOSITION OF ION THRUSTER EFFLUENTS ON SERT II SPACECRAFT SURFACES

by John V. Staskus and Robert J. Burns
Lewis Research Center
Cleveland, Ohio

TECHNICAL PAPER proposed for presentation at
Eighth Electric Propulsion Conference sponsored by the
American Institute of Aeronautics and Astronautics
Stanford, California, August 31 - September 2, 1970

# DEPOSITION OF ION THRUSTER EFFLUENTS ON SERT II SPACECRAFT SURFACES

by John V. Staskus and Robert J. Burns

Lewis Research Center
Cleveland, Ohio

TECHNICAL PAPER proposed for presentation at

Eighth Electric Propulsion Conference sponsored by the
American Institute of Aeronautics and Astronautics
Stanford, California, August 31 - September 2, 1970

NATIONAL AERONAUTICS AND SPACE ADMINISTRATION

# DEPOSITION OF ION THRUSTER EFFLUENTS ON SERT II SPACECRAFT SURFACES

by John V. Staskus and Robert J. Burns
Lewis Research Center
National Aeronautics and Space Administration
Cleveland, Ohio



## Abstract

An experiment aboard the SERT II spacecraft to detect surface contamination by mercury ion thruster effluents is discussed. Two solar cell sensors were located adjacent to each thruster downstream from the exhaust plane. Sensor short circuit current was the contamination sensitive parameter. One sensor at $+60^{\circ}$ C was used for detection of sputtered thruster accelerator grid material (Mo), and the other sensor at $-40^{\circ}$ C was used for detection of propellant (Hg) in addition to molybdenum. Flight data indicates that contamination of both sensors was due to molybdenum. Contamination of the low temperature sensor by mercury was negligible. Radiation intensity transmitted by the contamination film was reduced to 50 percent of the incident intensity within 6 to 12 hr of thruster start-up.

## Introduction

The SERT II spacecraft was launched on February 3, 1970 from the NASA Western Test Range. The mission objective was endurance testing of a mercury electron bombardment ion thruster[1] for a minimum of 6 months. Two thrusters were operated one at a time with power provided by a solar cell array. The orbit was 1000 km, nearly circular, and inclined at $99^{\circ}$. The orbit was nearly sun synchronous so that the solar array was exposed to continuous sunlight for a minimum of 6 months.

This report discusses an experiment to monitor the contamination of spacecraft surfaces downstream from the exhaust plane of the SERT II ion thruster. Neutral propellant (Hg) and sputtered accelerator material (Mo) are possible contaminants. The subject is of interest because of the electrical, thermal, optical, and chemical effects ion thruster effluents can have on spacecraft surfaces and systems. Accumulation of metals, sputtered or condensed, could bridge insulators in solar arrays, power distribution systems, or adjacent thrusters. The affected system would suffer a reduction in performance or be rendered inoperative. Chemical reaction of thruster effluents, notably cesium, severely degrades insulation.[2] Thermal control of spacecraft is impaired by a contaminant coating on surfaces or by chemical reaction of the contaminant with the surface material. Opaque contamination of solar cell surfaces results in loss of spacecraft power.

The results of a study considering the above effects are discussed in Ref. 2. Contamination by mercury ion thruster propellant was treated theoretically in Ref. 3. Contamination by sputtered thruster material was also investigated experimentally in Ref. 4. The tests of Ref. 4 were performed in a 7.6 m diameter vacuum facility using a 1.5 m diameter mercury ion thruster and SERT II type contamination sensors. Independent investigations of accelerator grid erosion produced particle emission rates but neglected the spatial distribution of the escaping particles.

The SERT II experiment provides the first flight measurement of mercury ion thruster efflux contamination on nearby spacecraft surfaces. It also provides a comparison to determine the applicability of ground-based experiments to flight conditions. The flight data consisted of a voltage proportional to the solar radiation intensity transmitted by the contaminant film.

## Background

The experiment simulated solar array equilibrium temperatures at 1 and 2 AU. Calculations indicate that a solar array front surface temperature is approximately $60^{\circ}$ C at 1 AU and $-40^{\circ}$ C at 2 AU. Propellant condensation is possible whenever the arrival flux is greater than the evaporation rate shown in Fig. 1. The arrival flux at the SERT II sensors is calculated using the following formula.[5]

$$\mu = \nu_o \frac{xz}{2(x^2+y^2)}\left[\frac{x^2+y^2+z^2+r_o^2}{\sqrt{(x^2+y^2+z^2+r_o^2)^2-4r_o^2(x^2+y^2)}}-1\right] \quad (1)$$

$\mu$ arrival flux at sensors, atom/cm$^2$ sec

$\nu_o$ exit flux from thruster = $[(1/\alpha)-1]I_5/(\pi r_o^2 q)$ atom/cm$^2$ sec

x, y, z coordinates of sensor center with thruster accelerator grid center as the origin, Fig. 2

$r_o$ exhaust radius of thruster, 6.78 cm

$\alpha$ propellant utilization efficiency, 0.77

$I_5$ ion beam current, 0.253 A

q unit charge, $1.6\times10^{-19}$ C

The arrival flux is found to be $5.62\times10^{13}$ (Hg atom)/(cm$^2$ sec) for the $-40^{\circ}$ C sensor (low temperature sensor) and $5.39\times10^{13}$ (Hg atom)/(cm$^2$ sec) for the $+60^{\circ}$ C sensor (high temperature sensor). The evaporation rate of mercury is $3\times10^{14}$ atom/cm$^2$/sec at $-40^{\circ}$ C. Therefore, condensation of mercury on the low temperature sensor at $-40^{\circ}$ C is critically dependent on the particle distribution. Mercury condensation will not occur on the high temperature sensor at $+60^{\circ}$ C.

The situation regarding molybdenum contamination is quite different. Ground tests reported in Ref. 4 resulted in deposition of accelerator grid material at 1 to 2.5 monolayers/hr (4.44 to $11.1\times10^{11}$ atom/cm$^2$ sec). Table I compares the ground test parameters with the SERT II parameters. A calculation using the relation[4]

$$\mu_1 = F\,\frac{If(3600)}{qA_o\sigma} \qquad (1)$$

where

$\mu_1$ arrival rate, monolayers/hr

F view factor, $(\mu/\nu_o)$, for cosine distribution from thruster exit to solar cell location, 0.0172 for low temperature sensor and 0.0165 for high temperature sensor

I ion beam current, 0.253 A

f fraction of primary ion current converted to charge exchange current, 0.00327

q $1.6\times10^{-19}$ C/unit charge

$A_o$ thruster cross-section area, 145 cm$^2$

$\sigma$ monolayer concentration (1 monolayer $\sim 1.6\times10^{15}$ atom/cm$^2$)

predicts an accumulation rate of approximately 1.37 monolayers/hr for SERT II due to sputtered molybdenum. Using this result and the data from Ref. 6 regarding the optical transmission of thin silver films, a graph of transmission versus time was generated, Fig. 3. Since data on the transmission of thin molybdenum films was not available, it was assumed that the transmission versus thickness for molybdenum was approximately the same as that for silver.

## Instrumentation

A high and low temperature sensor were mounted next to each other near the top of a large radiator facing the sun and a thruster. Systems 1 and 2 sensors were located adjacent to thrusters 1 and 2, respectively (fig. 4). Each contamination sensor consisted of a series-connected group of solar cells whose output was dissipated in a resistive load. Short circuit current is the parameter most sensitive to changes in input intensity and least sensitive to thermal variations. The load was, therefore, chosen to intersect the sensor characteristic on the short circuit current plateau (fig. 5).

The high and low temperature sensors were located at 63.7° and 61.6° from the beam axis and 36.8 and 33.8 cm, respectively, from the accelerator grid center, Fig. 4. The low temperature (LT) sensor was bonded to the radiator and the high temperature (HT) sensor was suspended on polyester cords for thermal isolation from the radiator. Behind each sensor was a thermistor to monitor the sensor temperature. A reflective blanket on the structure and insulating mounts reduced the thermal input from the sun and spacecraft. A more detailed description of the experiment is contained in the appendices.

## Results and Discussion

The contamination experiment began operation as soon as the spacecraft was oriented so that the contamination sensors faced the sun. Data was thus obtained prior to ion thruster operation. This data is shown in Fig. 6. Only data for system 2 is shown. However, the data from both systems were similar.

Fig. 6 shows a periodic oscillation of the sensor outputs at the orbit frequency (1/105 min). Part of the variation was determined to be due to shadowing of the sensors by the top of the thruster and a radio frequency interference experiment antenna (fig. 4). Shadowing occurred over 25 to 30 percent of the orbit in the southern hemisphere and was a result of the solar radiation being incident 26° from the orbit normal (fig. 7). As can be seen from the figure, no shadowing occurred over the northern hemisphere. The data also indicates that reflection from the top of the thruster to the sensors may have occurred over the northern hemisphere. This is evidenced by the leveling of the output voltage of the low temperature sensor at 40 and 140 min (fig. 6).

### System 2 Results

Thruster 2 was operated first. The thruster was brought to full thrust operation (253 mA beam current) in three steps. It was operated at 88 mA beam current for 19.4 hr, then 203 mA beam current for 6.8 hr and full beam for 11.7 hr. The thruster was then shut down in preparation for operation of the prime thruster. Data from the associated contamination experiment is shown in Figs. 8 and 9.

Figs. 8(a) and (b) show the transmission and temperature, respectively, for the low temperature sensor as a function of time for the 38 hr of thruster operation. The transmission is the normalized sensor output voltage multiplied by 100. Only the maximum voltage values, which occurred once per orbit, were used so that the oscillations due to shadowing and reflection are omitted. As is seen, the transmission decays rapidly with time, reaching 50 percent in 7.5 hr. The temperature was nearly constant at -40° C. The constant temperature eliminated the necessity for any temperature correction to the voltage data before comparing transmission data with the predicted graph of transmission versus time.

Figs. 9(a) and (b) show the transmission and temperature, respectively, for the high temperature sensor. As was the case with the low temperature sensor, transmission decreases rapidly with time, reaching 50 percent in 6.5 hr. The temperature data indicates that rather large temperature variations occurred. Detailed analysis of the data shows that the sensor temperature was lowest for the 20 to 30 min that the sensor was being shadowed over the southern hemisphere. The temperature was a maximum when the output voltage was a maximum (i.e., unshadowed) over the northern hemisphere and varied little from orbit to orbit. This elim-

inated any requirement for temperature correction to the voltage data before comparing transmission data with the predicted graph of transmission versus time. Comparison of the flight results, Figs. 8(a) and 9(a), with the results expected using Eqs. (1) and (2), Fig. 3, shows that the transmission decayed more rapidly than predicted. The reason for this is unknown, however, the prediction was obtained with the assumption that:

1. Eq. (1) gives an accurate description of the sputtered particle distribution.

2. f appearing in Eq. (2) is not a function of beam current.

3. The transmission of molybdenum thin films is the same as the transmission of silver thin films of the same thickness.

It is possible that one or more of the above assumptions are not valid.

Attempts were made to correlate the rate of transmission decay with ion beam current variations. However, as is seen in Figs. 8(a) and 9(a), the results showed wide variations that are not consistent with the view that the transmission should decrease proportionate to increasing ion beam current. The reasons for this are as yet unknown. Further tests are necessary to remove the inconsistency.

It is noted that, in general, the high temperature sensor transmission decayed more rapidly than the low temperature sensor transmission. This suggests a lower rate of contamination for the low temperature sensor. Consideration of the view factors, $\mu/\nu_0$, for the two sensors and the possible contamination mechanisms leads one to expect just the opposite to occur. The decay rate of the low temperature sensor transmission as a result of molybdenum accumulation, should be slightly higher than the rate for the high temperature sensor transmission. The addition of any mercury deposits on the low temperature sensor should result in its transmission decaying even more rapidly than the high temperature sensor transmission.

Further investigation is required to produce a satisfactory explanation for the discrepancy between the high and low temperature sensor contamination rates. However, it was concluded, from the fact that the decay rate of the low temperature sensors was not greater than the decay rate for the high temperature sensors, that no significant Hg contamination occurred.

When the thruster was initially turned on, the temperatures of the high and low temperature sensors decreased for about 40 hr. The temperatures then began increasing (fig. 10). The temperature variations were concluded to be due to the deposition of material on the sensors. The deposits initially caused small decreases in the solar absorptance $\alpha$, and this caused the sensor temperatures to decrease. As the deposit thickness increased, more rapid decreases in the emittance $\epsilon$, were obtained. The resultant increase in the absorptance-emittance ratio $\alpha/\epsilon$, caused the temperature of the sensors to increase. As Fig. 10(b) shows, the high temperature sensor temperature increased following thruster 2 shut down. This was due to a gradual decrease in the solar incidence angle from its initial value of $26^{\circ}$.

## System 1 Results

Figs. 11 and 12 show the transmission and temperatures as a function of time for the system 1 contamination sensors after thruster 1 startup. The thruster was operated at 94 mA beam current for 3.9 hr and 203 mA beam current for 1.93 hr. Operation then continued at full beam (253 mA) beyond the lifetime of the contamination experiment. The results obtained are similar to those obtained for system 2. The transmission decreased 50 percent in 12 and 8.8 hr for the low and high temperature sensors, respectively. As with system 2, the low temperature sensor transmission decayed slower than the high temperature sensor transmission and both decayed faster than predicted. Also, the system 1 results showed the same wide variation with ion beam currents as obtained with system 2.

The decay rates for the system 2 sensors were initially higher than those of the system 1 sensors. It was concluded that the system 2 sensors were being contaminated at a slightly higher rate. The accelerator grid sputtering rate is dependent on the flux of ions impinging on the grid. The accelerator drain current is a measurement of this flux. The thruster data indicated that the system 2 accelerator drain current was 1.75 mA compared to 1.60 mA for system 1. This is consistent with the higher contamination rate of the system 2 sensors compared to the system 1 sensors.

## Conclusion

Flight data showed considerable contamination. Contamination thickness reached 50 percent opacity in 7.5 to 12 hr for the sensors at $-40^{\circ}$ C and 6.5 to 8.8 hr for the sensors at $+60^{\circ}$ C. It was concluded that the contamination was caused by sputtered ion thruster grid material (molybdenum). Contamination by neutral propellant (mercury) was negligible. Analysis indicated that the high temperature sensors' transmission should decay slower than the low temperature sensors' transmission. The apparent discrepancy between the contamination rate of the low temperature sensor and that of the high temperature sensor has not yet been explained.

Attempts were made to correlate the contamination rates with thruster operating parameters. No consistent correlations could be obtained. Thus, predictions of contamination rates from thruster operating parameters and receptor location requires further investigation of thruster efflux distribution. Data on the transmission of molybdenum thin films is needed. With this data it may be possible to detect differences in contamination rate attributable to different thruster beam currents.

## Appendix A

### Sensors

The contamination sensors were basically groups of series-connected solar cells. The low temperature sensor consisted of 10 1×2 cm silicon N on P solar cells. The 0.033 cm thick cells had a base resistivity of 2 ohm-cm. The short circuit current was 65 mA ±5 percent at 25° C with one solar constant radiation input. The temperature coefficient of the short circuit current was no greater than 0.1 mA/°C. The cover glasses were 0.051 cm 7940 fused silica with a standard blue coating; adhesive was RTV 602. Two adjacent rows of cells were fixed to a 0.013 cm insulating sheet which was then bonded to a 0.13 cm stainless steel substrate. This assembly was then bonded to the radiator of the structure. The high temperature sensor consisted of 3 rows of 7 cells each. The materials and assembly were the same as the low temperature sensor's. The high temperature sensor contained more solar cells than the low temperature sensor since it was required to produce the same output at a higher temperature. Cell efficiency decreases with increasing temperature.

Four telemetry channels were required for each experiment. These were used to monitor the outputs from the high and low temperature sensors as well as sensor temperatures. Each parameter was sampled every 4 min and recorded as 0 to 61 "counts" for a 0 to 5 V telemetry voltage (0.082 V/count). The sensor output consisted of the voltage produced across a load resistor in series with the sensor (fig. 13). The resistor was chosen such that its load line intersected the sensor I-V characteristic on the portion proportional to short circuit current (fig. 5). Short circuit current was chosen as the sensitive parameter because it is most sensitive to variations in incident radiation intensity and least sensitive to temperature changes. The output was routed directly to the telemetry system with no intervening signal conditioning.

Temperature compensation was not necessary since the sensor's temperature varied slowly compared to the rate of contamination and the effect on the output was small. The temperature would have to change by 11° C before the output voltage variation would exceed the resolution of the telemetry system. Each sensor did, however, have a thermistor mounted behind it to monitor temperature changes. Thermistors for the temperature ranges of 0° to 80° C and -75° to -30° C were required. Temperature measuring circuitry is shown in Fig. 14. It should be noted that the temperature indicated by the thermistor was probably lower than the front surface of the solar cell cover glass. This is because 2.8 and 4.1 mm of glass, adhesives, silicon and metal separated the thermistor from the glass front surface. Calculations indicated the difference to be on the order of 2° to 3° C. The effect on the accumulation of sputtered molybdenum on the sensors should be negligible but it does require that the arrival rate of neutral mercury be approximately $5\times10^{14}$ atom/cm$^2$/sec rather than $3\times10^{14}$ atom/cm$^2$/sec before mercury accumulation occurs.

## Appendix B

### Structure

The experiment structure is an open rectangular pyramid of riveted aluminum construction (fig. 15). It consists primarily of a 27.9 cm by 50.8 cm plate which is oriented perpendicular to the top of the spacecraft and facing the sun (fig. 4). This plate serves as a radiator for the low temperature sensor and provides a support structure for both sensors. The sensors are mounted next to each other near the top of the radiator. The low temperature sensor is dispersed from the ion beam axis by 61.6° and is 33.8 cm from the center of the thruster accelerator grid. The high temperature sensor is 63.7° from the beam axis and 36.8 cm from the grid center. The low temperature sensor is bonded directly to the radiator and the high temperature sensor is thermally isolated from the radiator. Isolation is achieved by suspending the sensor behind a hole cut in the radiator.

Suspension of the high temperature sensor is provided by 24 lb, 480 filament, Dacron cord, Fig. 16. Dacron was chosen for its low thermal conductivity, high strength, and acceptable creep properties. Provision was made for periodic manual tightening of the suspension prior to flight to compensate for relaxation of the Dacron with time under load.

Thermal conduction from the spacecraft is minimized by mounting the experiment on fiberglass cylinders, Fig. 17. Thermal radiation from the sun and top of the spacecraft is minimized by covering the front of the radiator and one side of the structure with a reflective blanket. The blanket is composed of 20 layers of randomly wrinkled, aluminized, 0.0038 mm mylar with two cover sheets of 0.013 mm aluminized Kapton. A final 0.13 mm aluminized Kapton front cover provides support and protection for the blanket. The mylar is wrinkled to minimize the contact between sheets and prevent heat transfer by conduction. To prevent electrostatic charge accumulation on the aluminized surfaces, a multi-fingered aluminized Kapton strap attached to each layer of the blanket provides a ground circuit to the spacecraft. The materials and fabrication techniques used were similar to those used to build the Apollo Lunar Module multilayer insulation blanket.[7] A complete experiment weighed 2.1 kg.

Structural surfaces not covered by the thermal blanket were painted with Black Kemacryl having an emittance of 0.88. The rear surface of the high temperature sensor was 85 percent aluminum foil tape and 15 percent Black Kemacryl to maintain it at approximately +55° C.

Temperature predictions for various thermal control methods were made with a 32 node analytical model of the contamination experiment using the Chrysler Improved Numerical Differencing Analyzer (CINDA) program. Heat interchange between the superinsulating blanket and the main structure was computed as a radiation conductor using an effective emittance of 0.01. Radiation losses to the environment were tailored to

account for the side blockage due to the wrap-around of the blanket. The model was calibrated against experimental data obtained in the solar simulation qualification and flight acceptance tests. The data was used to analytically adjust the conductance paths to the high temperature sensor (heat conducted through the Dacron cords) as well as the heat loss through the mounting bolts. The flight temperature predictions were generated using the analytical model coupled to the analytical model of the thruster. Environmental heating was limited to solar and Earth thermal to the sun side and Earth thermal to the shade side. Albedo heating was neglected. Radiation heat interchange between the thruster and both of the sensors was included in the model. The shading of the insulating blanket by the thruster was also included. Using this model, the temperature predictions along with initial flight results are given in Table 2.

## References


1. Kerslake, W. R., Byers, D. C., and Staggs, J. F., "SERT II Experimental Thrustor System," Paper 67-700, Sept. 1967, AIAA, New York, N.Y.

2. Hall, D. F., "Evaluation of Electric Propulsion Beam Divergence and Effects on Spacecraft," Rep. 08965-6013-RO-00, Sept. 1969, TRW, Inc., Redondo Beach, Calif.

3. Staggs, J. F., Gula, W. P., and Kerslake, W. R., "The Distribution of Neutral Atoms and Charge-Exchange Ions Downstream of an Ion Thrustor," Paper 67-82, Jan. 1967, AIAA, New York, N.Y.

4. Richley, E. A. and Reynolds, T. W., "Condensation on Spacecraft Surfaces Downstream of a Kaufman Thruster," TM X-52746, 1970, NASA, Cleveland, Ohio.

5. Lozgachev, V. I., "Distribution of Molecular Flow on a Surface During Evaporation in Vacuum," Soviet Physics - Technical Physics, Vol. 7, No. 8, Feb. 1963, pp. 736-744.

6. Holland, L., Vacuum Deposition of Thin Films, John Wiley & Sons, Inc., New York, 1956, p. 245.

7. Bartilucci, A., Lee, E., and Tawil, M. N., "LM Passive Thermal Design and Test," Paper 68-748, June 1968, AIAA, New York, N.Y.


| | Grount test[4] | SERT II |
|---|---|---|
| Thruster radius, R, m | 0.75 | 0.068 |
| Beam current density, $A/m^2$ | 5.7 | 17.2 |
| Neutral mercury efflux rate, atoms/$cm^2$ sec | $3.6\times10^{15}$ | $3.27\times10^{15}$ |
| Distance from thruster exit to experimental solar cells, L, m | 4.21 | 0.353 |
| L/R ratio | 5.63 | 5.19 |
| Angle from thruster center-line to solar cell experiment, deg | 57 | 62.6 |
| View factor; ratio of flux arriving at solar cell to flux leaving thruster exit, $\mu/\nu_o = F$ | 0.019 | 0.0168 |

TABLE 1 COMPARISON OF SERT II PARAMETERS WITH GROUND TEST PARAMETERS

| Sensor | Temperature, °C | |
|---|---|---|
| | Predicted | Achieved |
| LT no. 1 | -54.4 | $-37.6\ ^{+4.2}_{-1.4}$ |
| HT no. 1 | 57.2 | $61.3\ ^{+4}_{-1.2}$ |
| LT no. 2 | -54.4 | $-40.8\ ^{+4.2}_{-1.4}$ |
| HT no. 2 | 57.8 | $62.8\ ^{+4}_{-1.2}$ |

TABLE 2 COMPARISON OF PREDICTED SENSOR TEMPERATURES WITH FLIGHT RESULTS

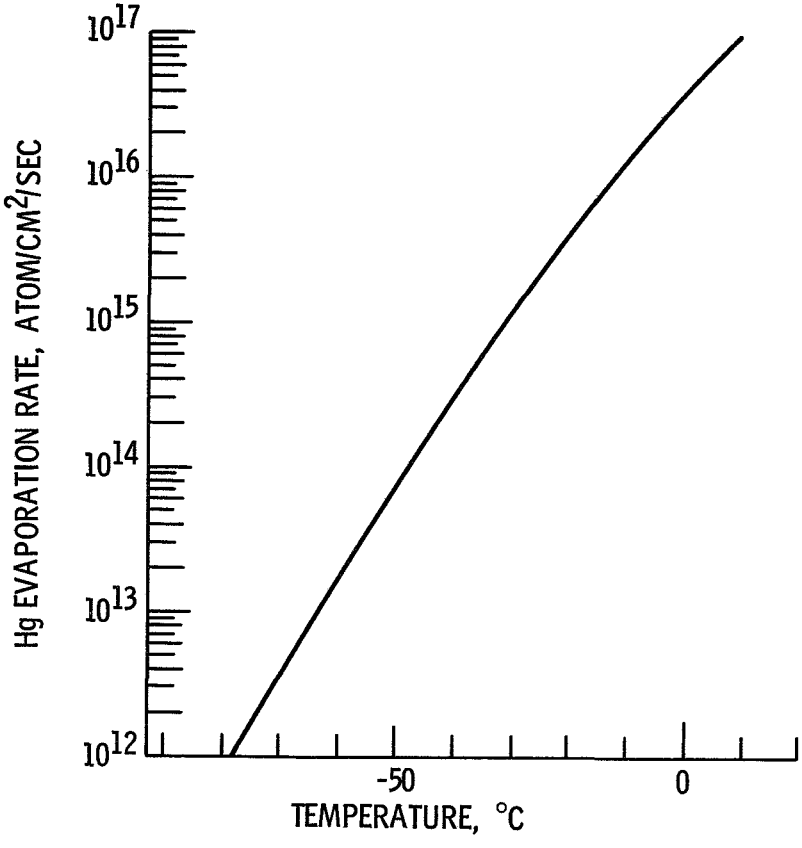


Figure 1. - Mercury evaporation rate as a function of temperature.

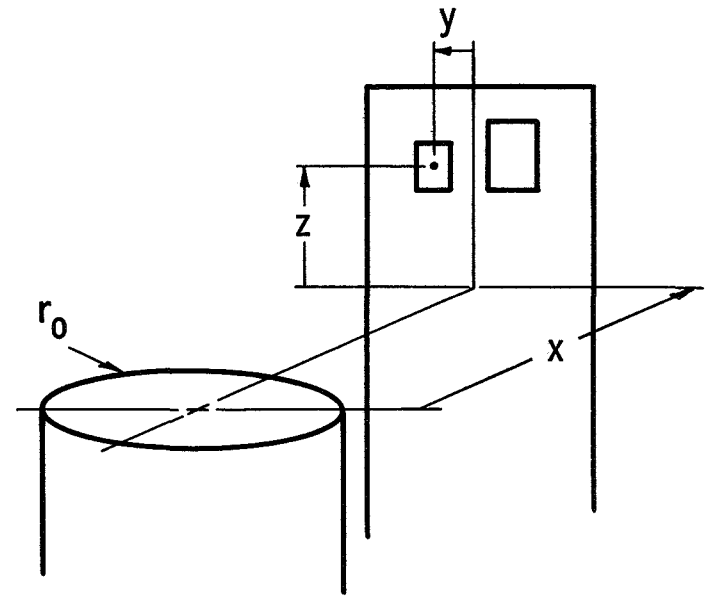


| SENSOR | COORDINATE, CM | | |
|---|---|---|---|
| | x | y | z |
| LOW TEMPERATURE | 29.39 | 4.67 | 16.1 |
| HIGH TEMPERATURE | 30.96 | 3.58 | 15.28 |

Figure 2. - Coordinate definition and values for use in equation (1).

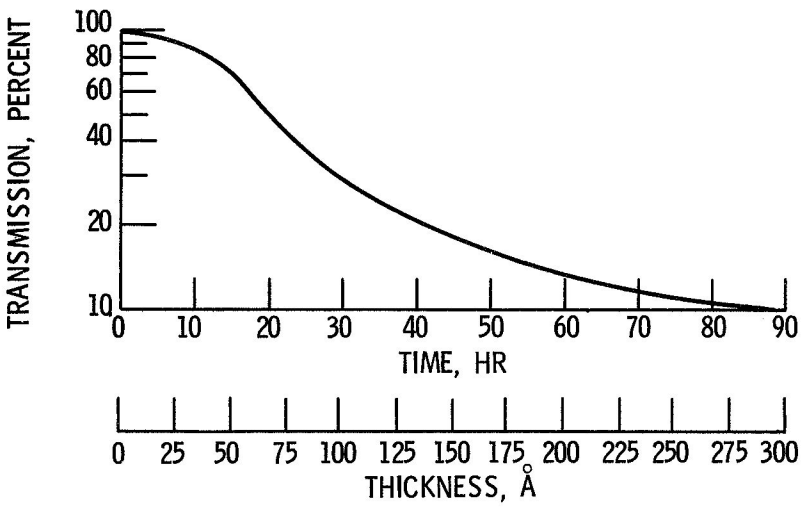


Figure 3. - Predicted transmission as a function of time using equations (1) and (2) and reference 5. Thickness scale taken directly from reference 5.

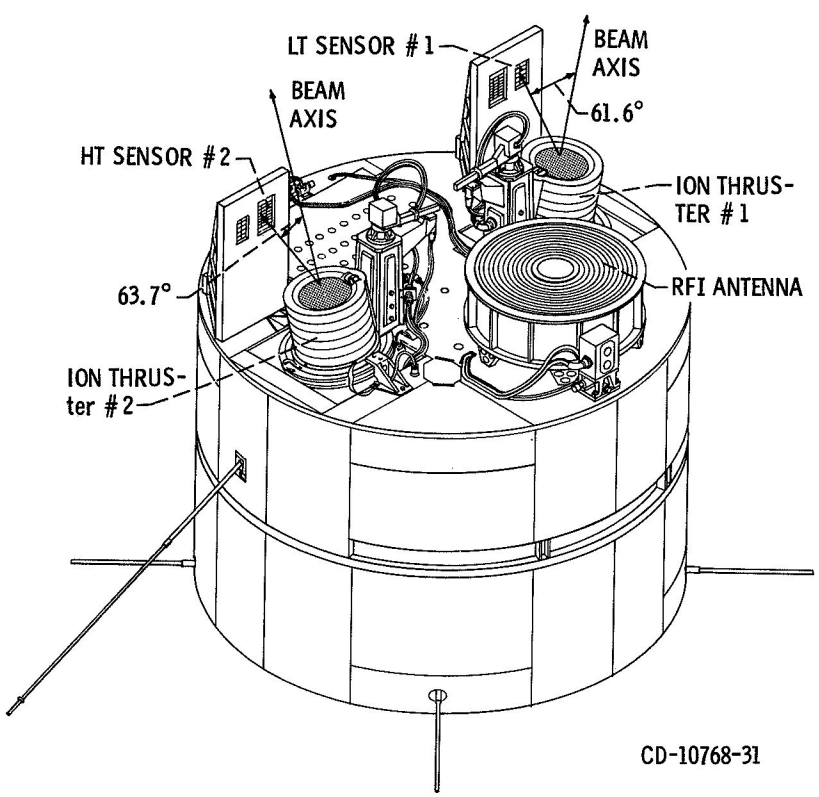


Figure 4. - SERT II spacecraft showing contamination sensor locations.

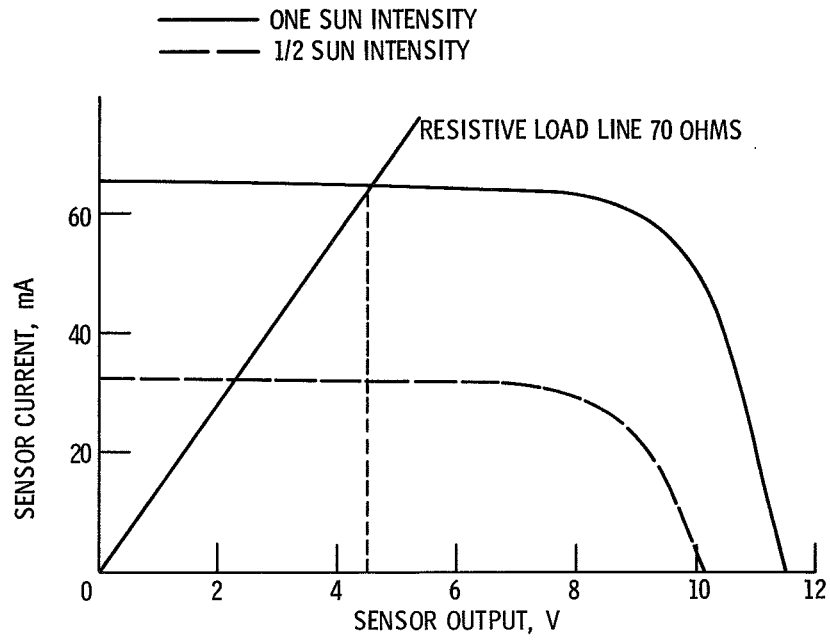


Figure 5. - High temperature sensor characteristic.

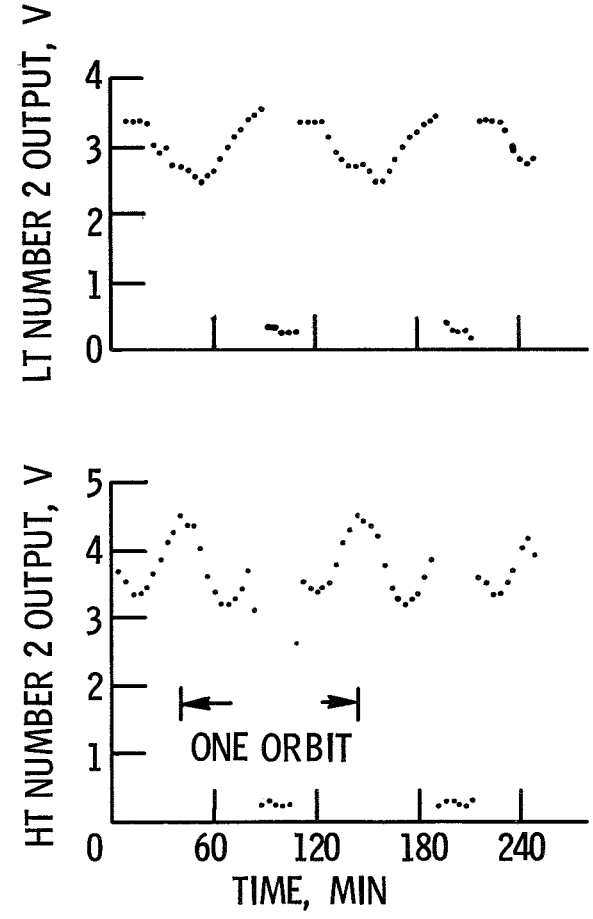


Figure 6. - Contamination sensor output voltages prior to thruster start-up.

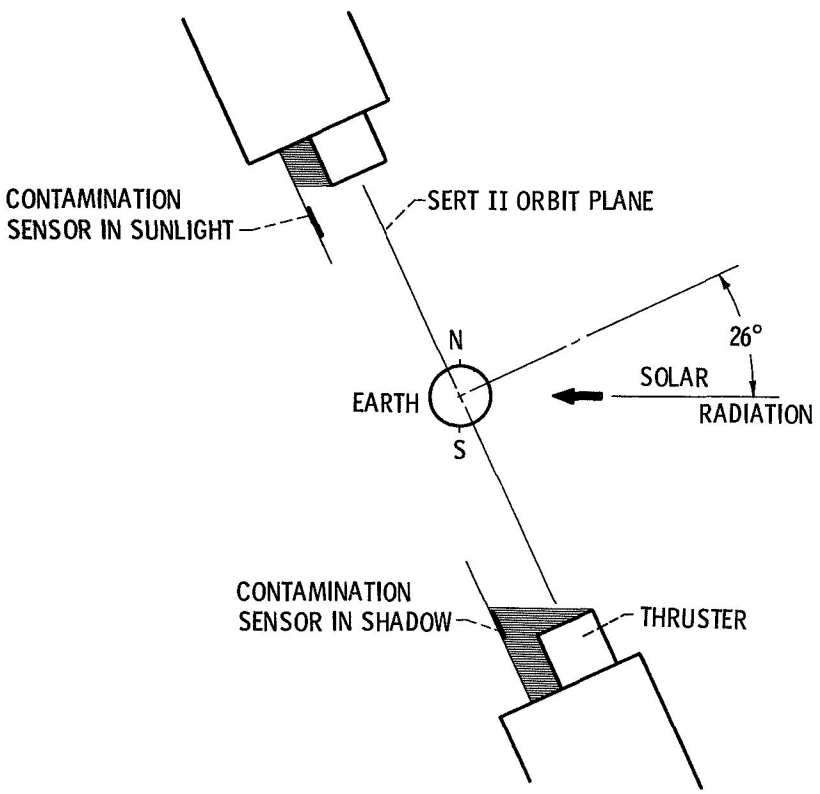


Figure 7. - Illustration of ion thruster shadowing contamination sensor over part of southern hemisphere.

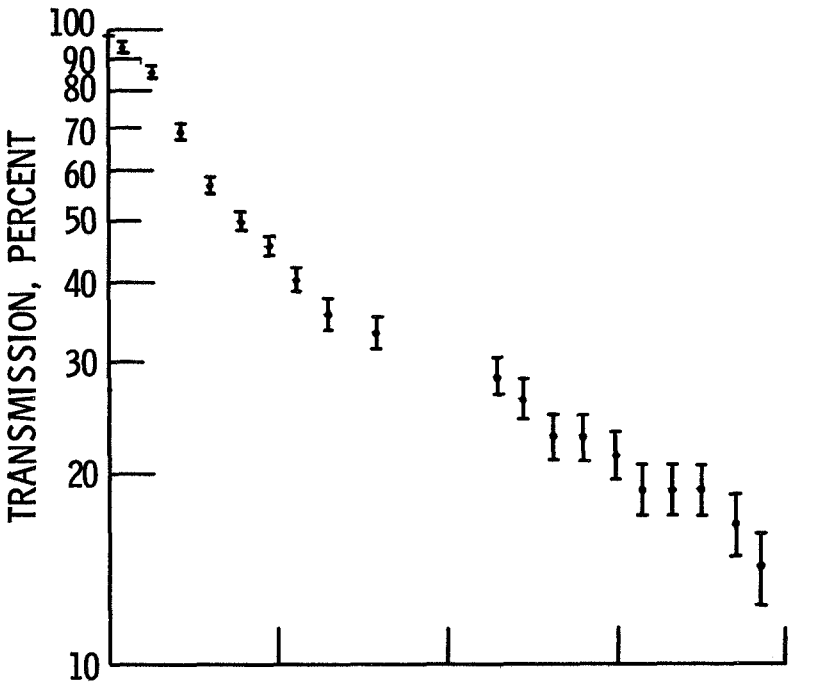


(A) TRANSMISSION.

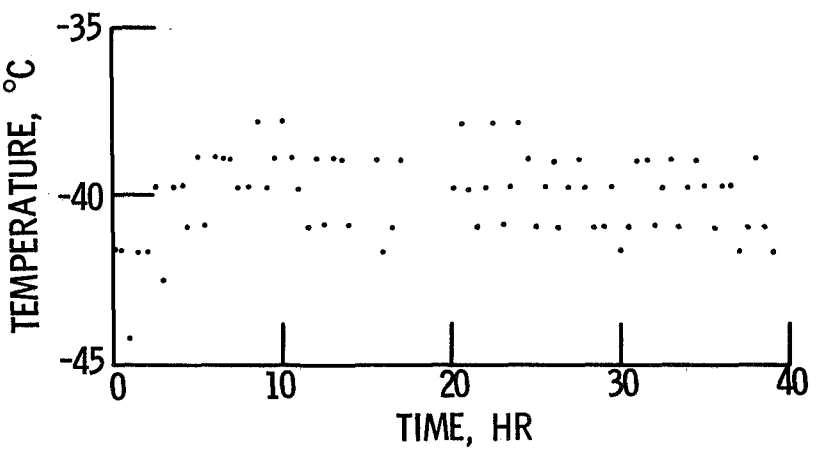


(B) TEMPERATURE.

Figure 8. - System 2 low temperature sensor transmission and temperature as a function of time from thruster start-up.

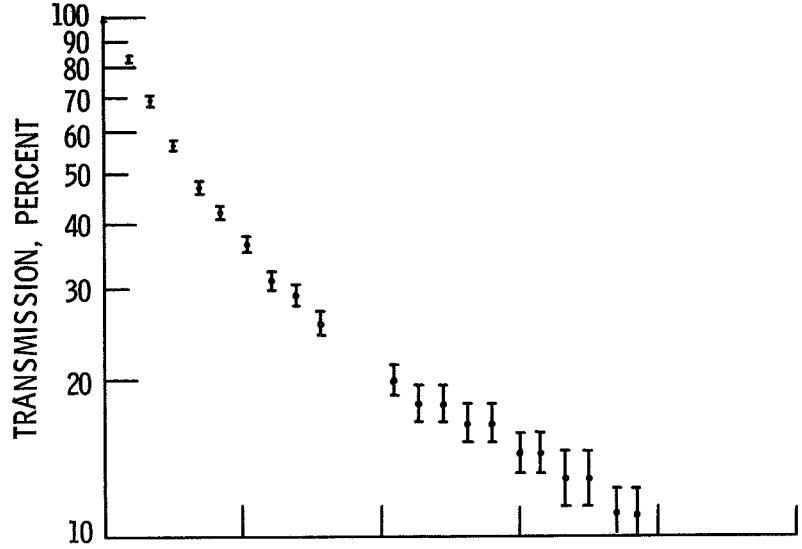


(A) TRANSMISSION.

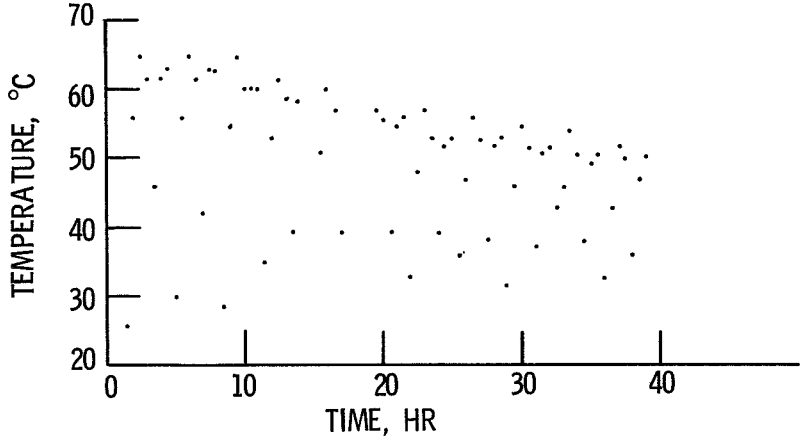


(B) TEMPERATURE.

Figure 9. - System 2 high temperature sensor transmission and temperature as a function of time from thruster start-up.

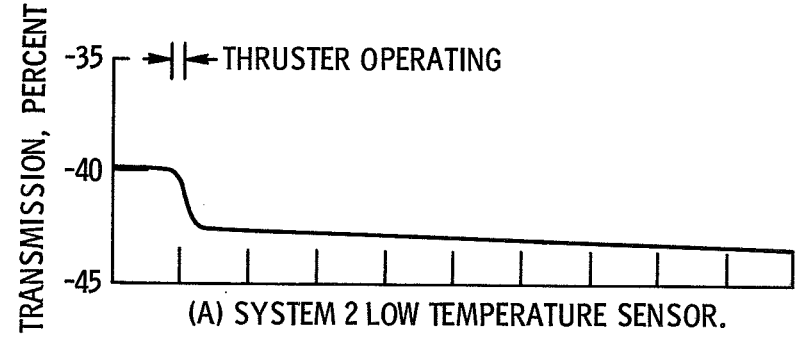


(A) SYSTEM 2 LOW TEMPERATURE SENSOR.

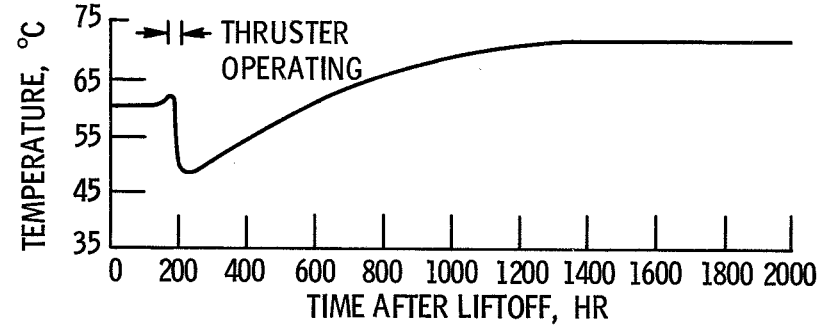


(B) SYSTEM 2 HIGH TEMPERATURE SENSOR.

Figure 10

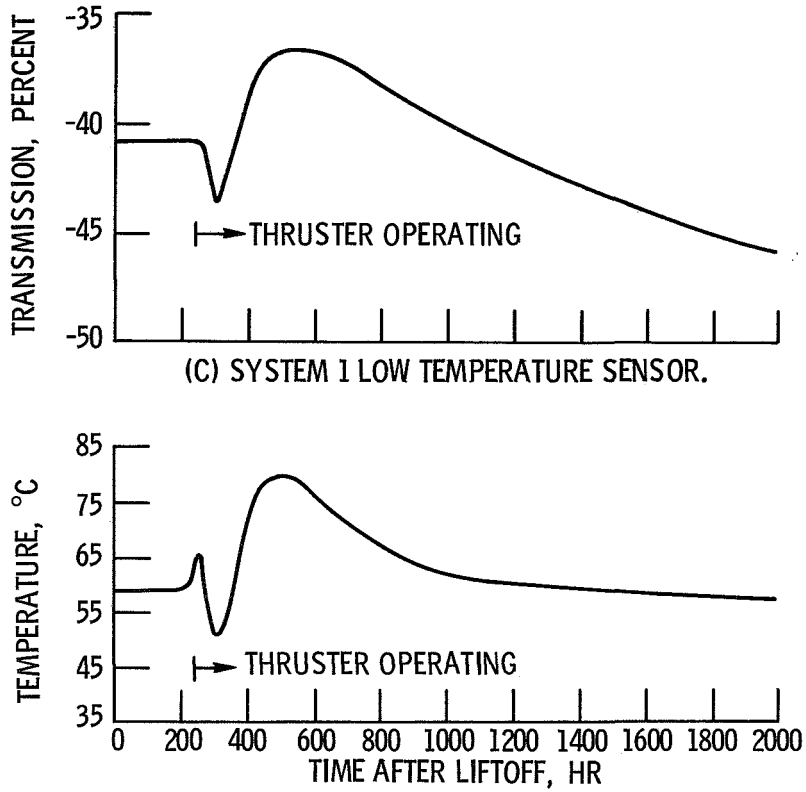


Figure 10. - Sensor temperatures as a function of time from SERT II lift off.

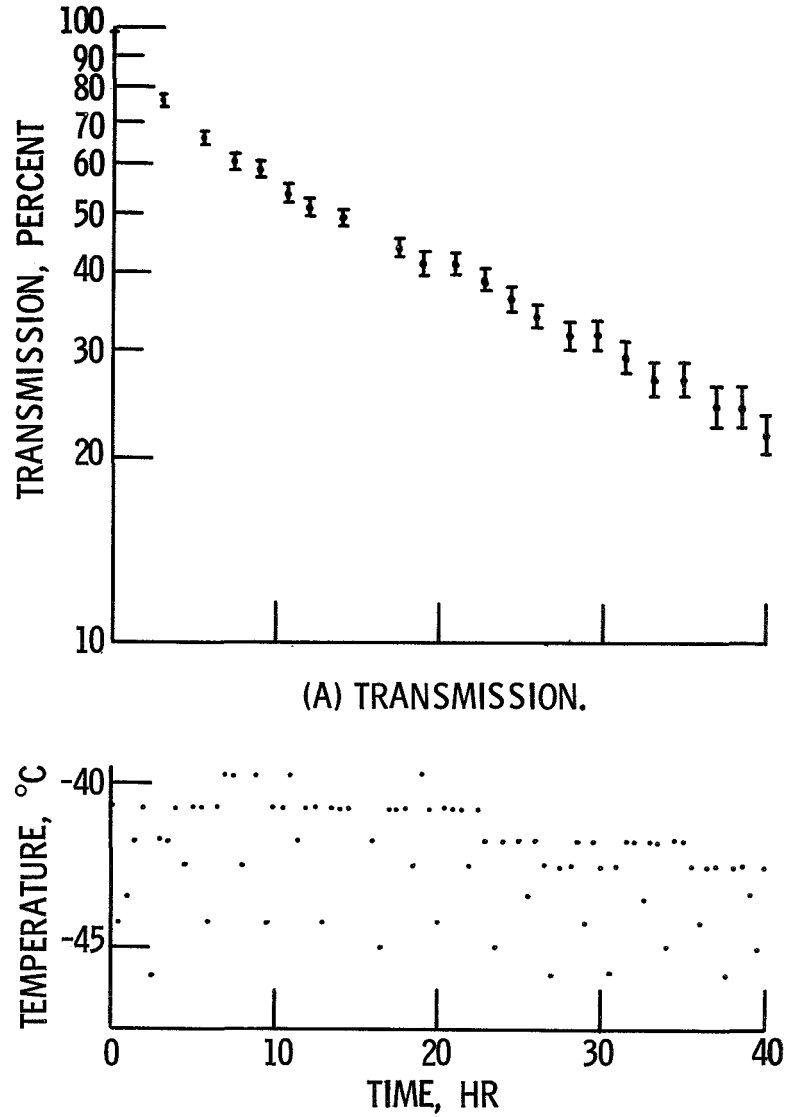


Figure 11. - System 1 low temperature sensor transmission and temperature as a function of time from thruster start-up.

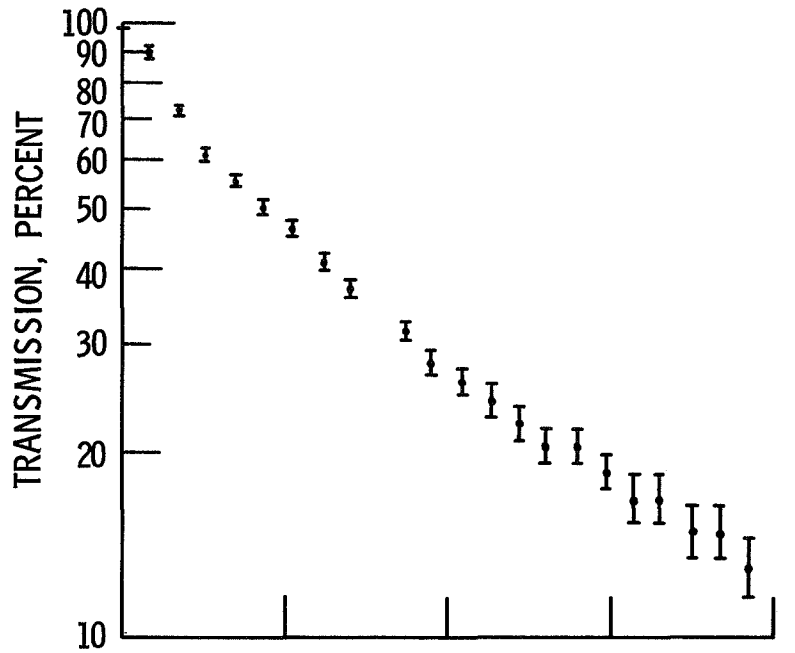


(A) TRANSMISSION.

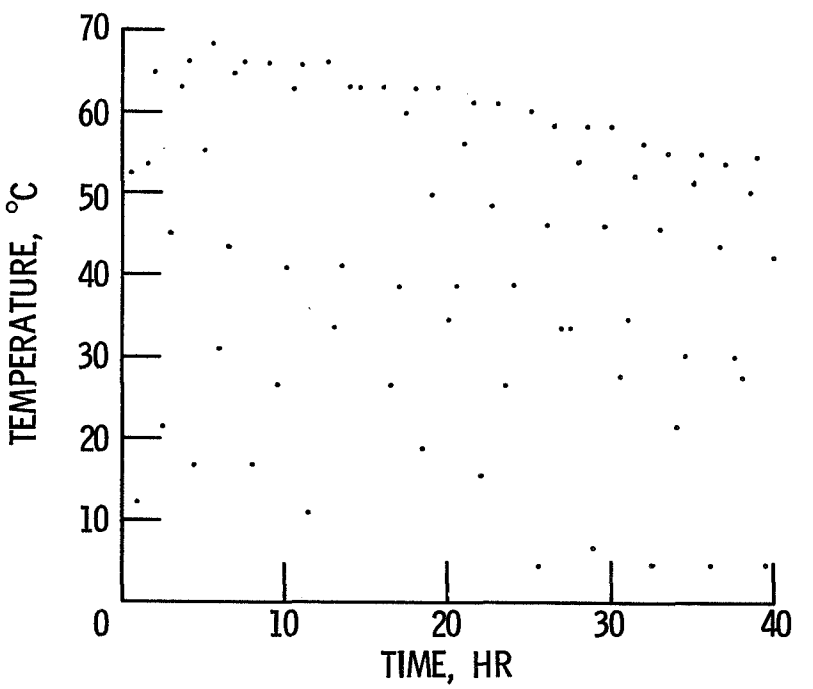


(B) TEMPERATURE.

Figure 12. - System 1 high temperature sensor transmission and temperature as a function of time from thruster start-up.

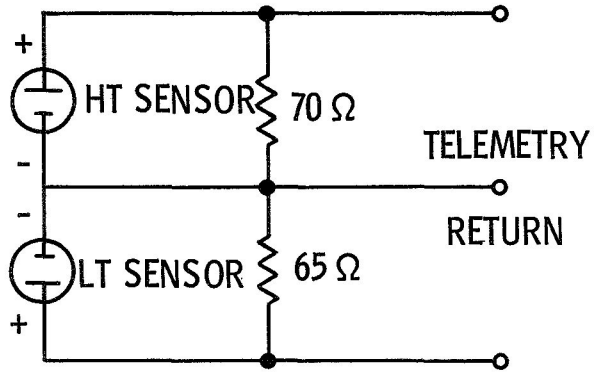


Figure 13. - Sensor circuits.

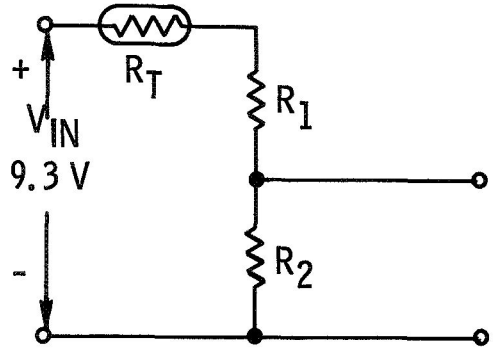


| SENSOR | $R_1$, Ω | $R_2$, Ω | $R_T$, TYPE |
|---|---|---|---|
| LT | 6.98 K | 15 K | FENWAL GB25JM6 |
| HT | 13.7 K | 30 K | GULTON 58CX1 |

Figure 14. - Temperature measurement circuits.

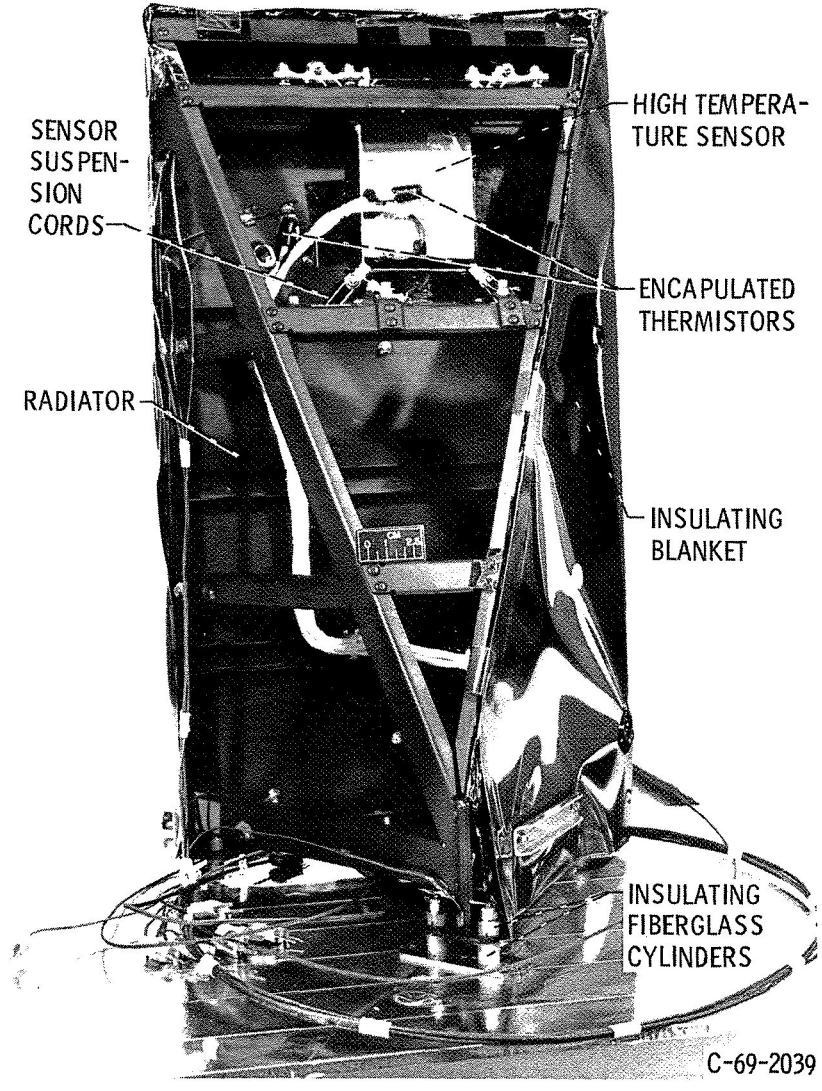


Figure 15. - Contamination experiment structure.

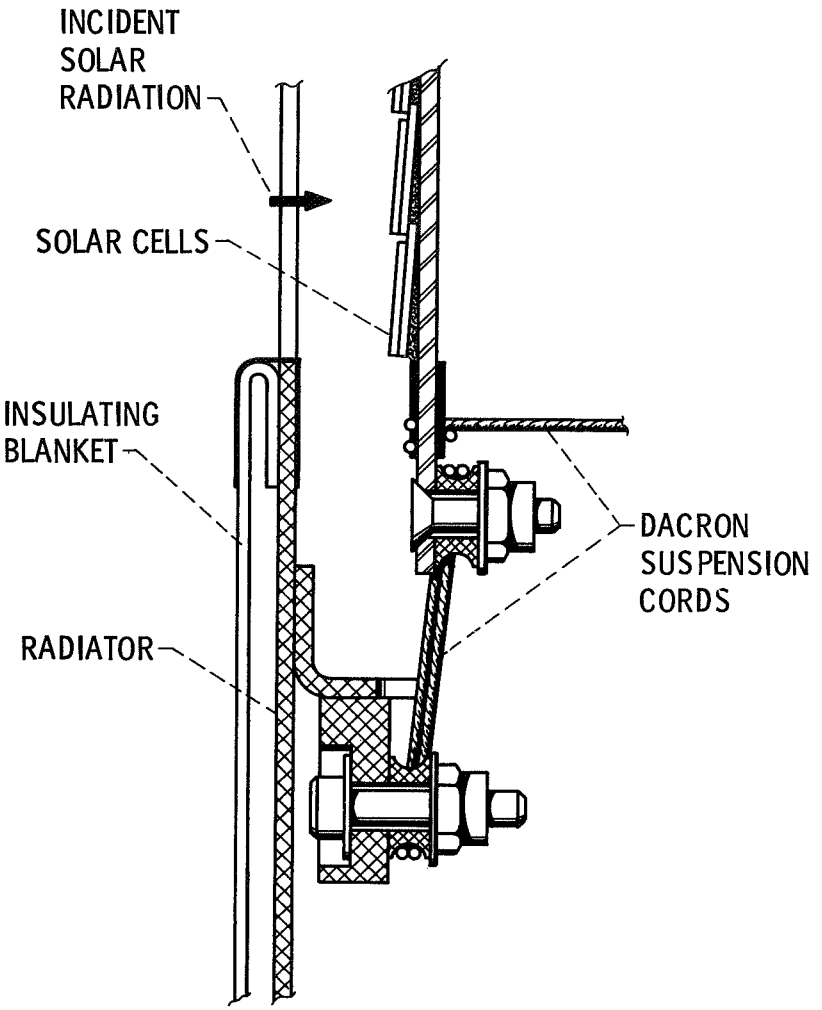


Figure 16. - High temperature sensor mounting detail.

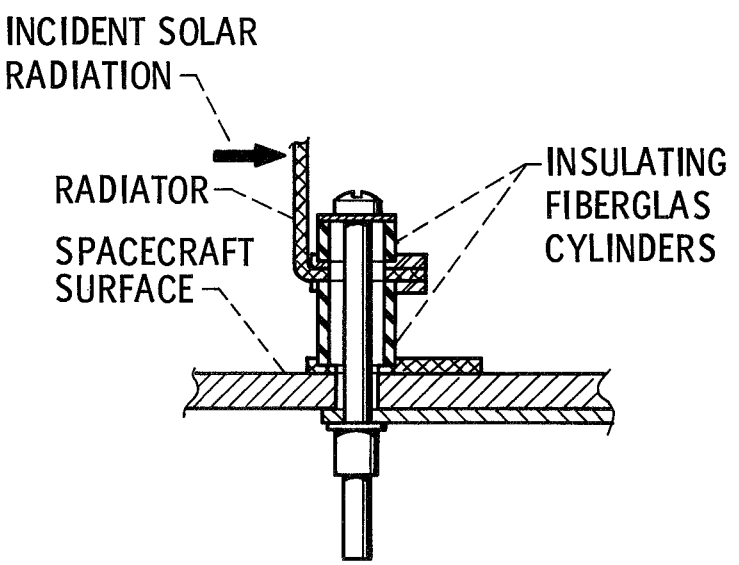


Figure 17. - Experiment mounting.